
Oral presentation | Incompressible/compressible/hypersonic flow

Incompressible/compressible/hypersonic flow-III

Thu. Jul 18, 2024 10:45 AM - 12:45 PM Room D

[10-D-01] A Space-Marching Immersed-Boundary Method for Near-Field Sonic Boom Simulation

*Rei Yamashita¹ (1. The University of Tokyo)

Keywords: Space marching method, Immersed boundary method, Sonic boom, Supersonic flow

A Space-Marching Immersed-Boundary Method for Near-Field Sonic Boom Simulation

Rei Yamashita*

Corresponding author: reiyamashita@g.ecc.u-tokyo.ac.jp

* The University of Tokyo, JAPAN.

Abstract: This study realizes fast three-dimensional simulations of supersonic flows around complex geometries in a space marching manner. Thus far, complex geometries have not been considered using a space marching method which restricts grid topology. In this study, a novel immersed boundary method on Cartesian grids is developed under requirement of supersonic conditions for space marching. The axisymmetric and three-dimensional steady Euler equations are respectively solved to simulate flows around a complex axisymmetric geometry and a delta wing body used in the American Institute of Aeronautics and Astronautics (AIAA) sonic boom prediction workshops. The computational results show that all waves emanating from complex geometries are highly resolved over the radial distance several times the body length. The pressure signatures are comparable to those obtained in the previous simulations using time marching methods and in wind tunnel experiments. The three-dimensional simulation of flows around a delta wing body that includes the grid generation takes less than 100 s on a laptop. These results indicate that fast simulations of supersonic flows with complex geometries are enabled by employing a space marching method in combination with an immersed boundary method.

Keywords: Space Marching Method, Immersed Boundary Method, Computational Fluid Dynamics, Sonic Boom.

1 Introduction

Shock waves emanating from a supersonic aircraft cause explosive sound on the ground, which is known as sonic boom [1]. Sonic boom strength must be mitigated for enabling overland supersonic flight that has been restricted. Therefore, approaches to design of low sonic boom supersonic aircraft have been developed for decades. They generally require parametric studies that include computational fluid dynamics (CFD) analysis.

For sonic boom prediction, three-dimensional CFD simulations must be applied in the near field around an aircraft, extending to a radial distance five to ten times the aircraft length [2]; thus, the computational cost is too high to cope with both accurate sonic boom prediction and efficient parametric studies. To address this issue, a space marching method [2, 3, 4, 5], instead of conventional time marching methods, has been applied. This is because sonic boom can usually be predicted under the assumption of supersonic flows everywhere. All information for supersonic flows propagates downstream, hence their flows can be solved by marching in space. For a space marching method, a spatially three-dimensional steady problem can be reduced to a spatially two-dimensional unsteady problem, leading to considerable reduction of computational cost. The latest three-dimensional CFD simulation [2] extending to a radial distance ten times the aircraft length took only a minute on a standard laptop when using an explicit space marching method. Furthermore, full-field simulation [6] of sonic boom over the entire flow field extending to the ground has successfully been performed in a space marching manner. The previous studies described above indicate that fast CFD simulations except for the vicinity of supersonic aircraft have been achieved by employing a space marching method. However, the restriction of supersonic conditions for space marching makes it difficult to consider complex geometries, even when inviscid flows are assumed; i.e., numerical simulations in the vicinity of a supersonic aircraft must be performed in a time marching manner, while still keeping high computational cost.

In this study, we newly propose an immersed boundary method [7, 8] in combination with a space marching method, which enables fast simulations involving complex geometries. For a space marching method, downstream data is calculated using only upstream data. However, both upstream and downstream data are conventionally used for applying immersed boundary conditions; thus, general immersed boundary methods are not applicable directly. Therefore, the objectives of this study are to develop a novel immersed boundary method that can be used with a space marching method and to realize near-field sonic boom simulations around complex geometries in a space marching manner.

2 Computational Method

A novel immersed boundary method in combination with an explicit space marching method in Cartesian coordinates is developed to consider complex geometries in steady supersonic flows. It is described in this section.

2.1 Governing Equations

The governing equations are the three-dimensional steady Euler equations in Cartesian coordinates (x, y, z) :

$$\frac{\partial E}{\partial x} + \frac{\partial F}{\partial y} + \frac{\partial G}{\partial z} = 0 \quad (1)$$

$$E = \begin{bmatrix} \rho u \\ \rho u^2 + p \\ \rho uv \\ \rho uw \\ (e + p)u \end{bmatrix}, F = \begin{bmatrix} \rho v \\ \rho uv \\ \rho v^2 + p \\ \rho vw \\ (e + p)v \end{bmatrix}, G = \begin{bmatrix} \rho w \\ \rho vw \\ \rho w^2 + p \\ (e + p)w \end{bmatrix} \quad (2)$$

where E is the vector of conservative variables for space marching. F and G are the flux vectors in the y and z directions, respectively. u , v , and w are the velocity components in the x , y , and z directions, respectively. ρ and p are the density and pressure, respectively. The total energy is calculated as

$$e = \frac{p}{\gamma - 1} + \frac{\rho}{2}(u^2 + v^2 + w^2) \quad (3)$$

where the ratio of specific heats for air is $\gamma = 1.4$. The system of the governing equations is closed by the equation of state as

$$p = \rho RT \quad (4)$$

where T is the temperature and the gas constant is $R = 287 \text{ J}/(\text{K}\cdot\text{kg})$.

2.2 Space Marching Method

Sonic boom can usually be predicted under the assumption of supersonic flows everywhere. All information for supersonic flows propagates downstream, hence their flows can be solved by marching in space. The governing equations given by Eq. (1) can be rewritten as

$$\frac{\partial E}{\partial x} = - \left(\frac{\partial F}{\partial y} + \frac{\partial G}{\partial z} \right) = R(E) \quad (5)$$

where x is the marching direction and acts like time which is evaluated in conventional time marching solvers. The vector of conservative variables, E , can be updated by only one marching sweep, in which the numerical fluxes F and G are calculated. Therefore, a spatially three-dimensional steady problem given by Eq. (1) can be reduced to a spatially two-dimensional unsteady problem given by Eq. (5), leading to considerable reduction of computational cost. A space marching solver can be formulated in the same way as conventional time marching solvers. In this study, we apply the third-order total variation diminishing (TVD) Runge-Kutta method [9] as

$$\begin{aligned} E^{(1)} &= E_i + \Delta x R(E_i) \\ E^{(2)} &= \frac{3}{4}E_i + \frac{1}{4}E^{(1)} + \frac{1}{4}\Delta x R(E^{(1)}) \\ E_{i+1} &= \frac{1}{3}E_i + \frac{2}{3}E^{(2)} + \frac{2}{3}\Delta x R(E^{(2)}) \end{aligned} \quad (6)$$

The numerical fluxes F and G can be calculated in the similar way as those evaluated in conventional numerical schemes. The third-order monotonic upstream-centered schemes for conservation law (MUSCL) [10] interpolation is employed with the minmod limiter. The AUSM⁺-up scheme [11] is used as an approximate Riemann solver. In a space marching method, the primitive variables are calculated from the

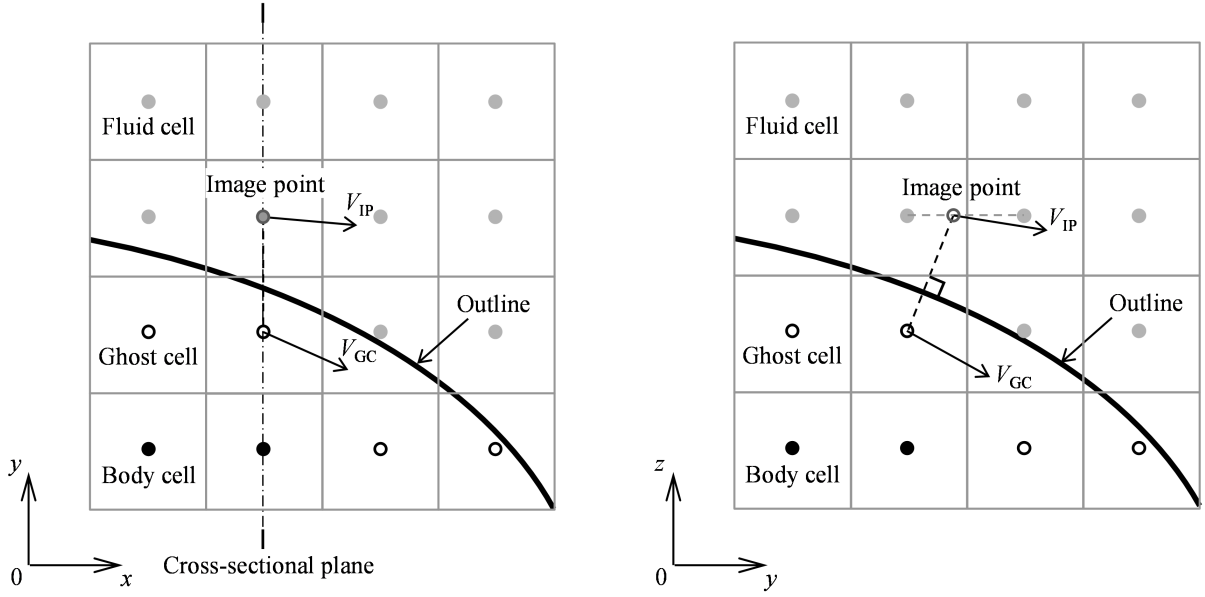


Figure 1: Immersed boundary method for space marching. Immersed boundary conditions are determined on a cross-sectional plane vertical to the x direction (left: side view, right: front view).

vector of conservative variables, $E = (e_1, e_2, e_3, e_4, e_5)^T$, as

$$\begin{aligned}
 p &= \frac{e_2 \pm \sqrt{e_2^2 - (\gamma^2 - 1)(2e_1e_5 - e_2^2 - e_3^2 - e_4^2)}}{\gamma + 1} \\
 u &= (e_2 - p)/e_1 \\
 v &= e_3/e_1 \\
 w &= e_4/e_1 \\
 \rho &= \frac{\gamma p}{\gamma - 1} \left(\frac{e_5}{e_1} - \frac{u^2 + v^2 + w^2}{2} \right)^{-1}
 \end{aligned} \tag{7}$$

where the plus and minus signs apply for subsonic and supersonic flows, respectively.

For explicit time marching methods, a time step is restricted due to Courant-Friedrichs-Lewy (CFL) constraint; i.e. a numerical information speed within one time step must be faster than a wave propagation speed. Conversely, for an explicit space marching method, grid topology is restricted due to CFL constraint as

$$\tan \theta < \min \left(\frac{\Delta y}{\Delta x}, \frac{\Delta z}{\Delta x} \right) \tag{8}$$

where θ can be approximated as the maximum shock wave angle. Under this constraint, computational grids used in a space marching method must be generated. The CFL constraint can be alleviated when using implicit solvers [4, 5]. However, their solvers require inner iterations which increase computational cost; i.e., the advantage of reduction in computational cost owing to space marching is diminished. Therefore, in this study, the explicit solver given by Eq. (6) is applied as in the previous study [2, 6], and computational grids are generated under consideration of the CFL restriction.

2.3 Immersed Boundary Method for Space Marching

For sonic boom prediction, fast CFD simulations except for the vicinity of supersonic aircraft have been achieved by employing a space marching method. However, the restriction of CFL and supersonic conditions makes it difficult to consider complex geometries in a space marching manner; i.e., numerical simulations in the vicinity of a supersonic aircraft must be performed in a time marching manner, while still keeping high computational cost. We therefore propose a novel immersed boundary method for space marching, which enables fast flow simulations with complex geometries.

Immersed boundary methods [7, 8] have been applied for considering complex geometries on Cartesian grids. Their usefulness has been confirmed in many previous simulations using time marching methods

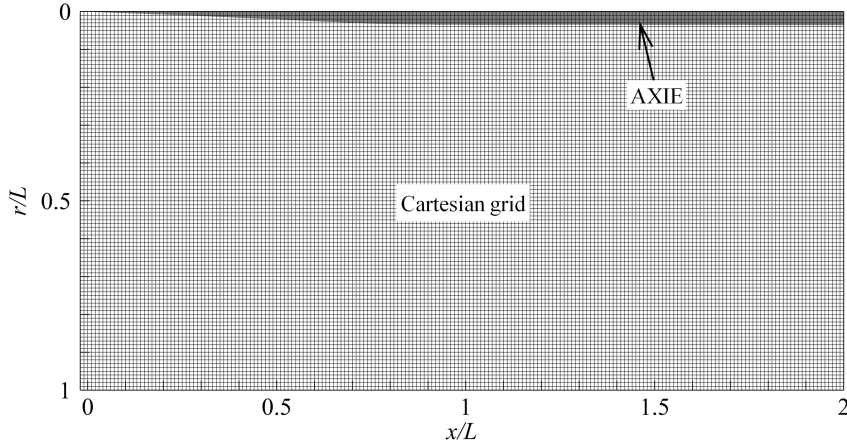


Figure 2: Coarse Cartesian grids in the vicinity of the AXIE model, shown every 10 points in all directions.

Table 1: Overview of Cartesian grids used for axisymmetric simulation of flows around the AXIE model.

Grid	Grid spacing		Number of grid points		Computational time [s]
	$\Delta x/L$	$\Delta r/L$	x direction	r direction	
Coarse	0.002		4511	5001	3.0
Medium	0.001		9021	10001	11.0
Fine	0.0005		18041	20001	42.6

[12, 13, 14]. Conversely, for space marching methods, they have not been applied to date. Figure 1 shows an overview of the immersed boundary method developed in this study. Grid cells are classified into body cells, fluid cells, and ghost cells inside the body adjacent to fluid cells. An immersed boundary condition is conventionally set using data at an image point that is allocated on the normal vector to the surface of a body. In a space marching method, downstream data needs to be updated using only upstream data; i.e., an immersed boundary condition must be made using only upstream data, without downstream data. Thus, a conventional immersed boundary method that uses downstream data cannot be directly applied for space marching solvers. In this study, we propose a novel immersed boundary method which can be used with a space marching method, as shown in Fig. 1. An immersed boundary condition at $x = x_i$ is calculated from data on a cross-sectional plane at $x = x_i$ as

$$\begin{aligned}
 \mathbf{V}_{GC} &= \frac{|\mathbf{V}_{IP}|}{|\mathbf{V}_{IP,t}|} \mathbf{V}_{IP,t} \\
 p_{GC} &= p_{IP} \\
 \rho_{GC} &= \rho_{IP}
 \end{aligned} \tag{9}$$

where \mathbf{V} denotes the velocity vector (u, v, w) . The subscripts GC and IP denote the ghost cell and the image point, respectively. The subscript t denotes the tangential vector to a body at $x = x_i$. An image point is set on a planar vector at $x = x_i$ that is normal to the cross-sectional outline of a body at $x = x_i$, as shown in Fig. 1. Computational accuracy of the method proposed above is lower than that of conventional immersed boundary methods because an image point is not allocated on a vector normal to the surface of a body. However, this disadvantage can be easily overcome by applying adequately fine grids which can be allowed for space marching. This is because a space marching method enables a spatially three-dimensional steady problem to be reduced to a spatially two-dimensional unsteady problem, leading to considerable reduction of computational cost. Thus, deterioration of resolution on immersed boundaries is trivial when applying a space marching method.

3 Validation and Evaluation

Numerical simulations were performed to demonstrate that complex axisymmetric (Sec. 3.1) and three-dimensional (Sec. 3.2) geometries can be resolved by the immersed boundary method for space marching which is proposed in Sec. 2.3.

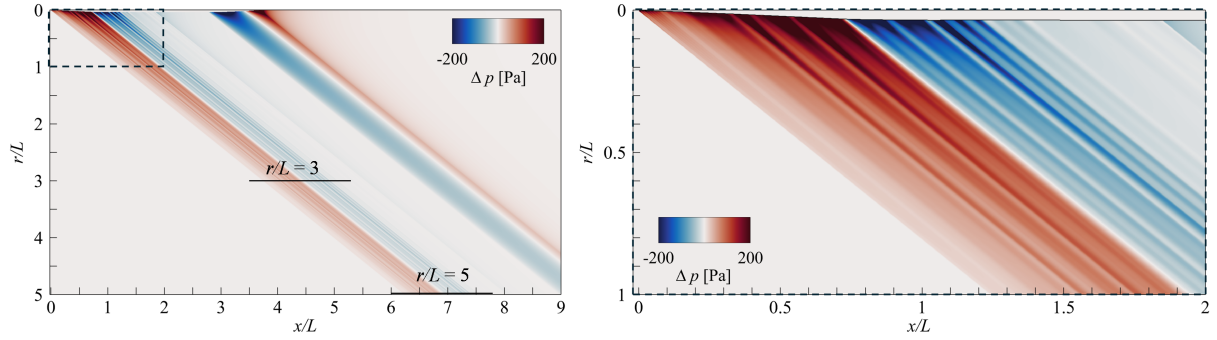


Figure 3: Overpressure distribution around the AXIE model that is considered as immersed boundaries in axisymmetric simulation using a space marching method (left: overall view, right: closeup view in the vicinity of the AXIE model).

3.1 Numerical Simulation of Flows around a Complex Axisymmetric Body

Multiple shock waves emanating from the Axisymmetric Equivalent Area (AXIE) [15] model were solved in this section. The AXIE model is an axisymmetric geometry with an area equivalent to the C25F [15] low sonic boom supersonic aircraft, which consists of wing, body, tail, nacelle, and flow-through engine. It was designed to recover a pressure signature at three times the body length under track of the C25F aircraft. The length of the AXIE model is $L = 32.92$ m. The AXIE model was used in the second American Institute of Aeronautics and Astronautics (AIAA) sonic boom prediction workshop (SBPW). The geometry data and computational results gathered from many participants in the SBPW are publicly available. Therefore, the AXIE model was selected as a test case to validate the accuracy of the immersed boundary method developed in this study. The computational conditions were the same as those used in the SBPW. The freestream Mach number was set to 1.6, and zero angle of attack was assumed.

The flow field around the AXIE model was modeled by the axisymmetric Euler equations on the square Cartesian grids. The computational domain in the streamwise (x) and radial (r) directions ranges over $x/L = -0.02-9$ and $r/L = 0-10$, respectively. The AXIE model was considered by the immersed boundary method described in Sec. 2.3. The boundary at $r = 0$ was evaluated under the assumption of axisymmetry. The boundary at $r = r_{\max}$ was evaluated as zeroth order extrapolation. The boundary condition at $x = x_{\min}$, which is equivalent to the initial condition in the simulation using a space marching method, was set to the freestream condition. The boundary condition at $x = x_{\max}$ was not required for space marching solvers. Figure 2 shows the computational grid in the vicinity of the AXIE model. The computations were made on the coarse, medium, and fine grids which were used for the grid convergence study. Table 1 shows the overview of the computational grids and the computational time on a laptop with Intel Core™ i7-1255U (10 cores). The simulation using the fine grids with approximately 0.36 billion points took only 42.6 s. This demonstrates that fast axisymmetric flow simulations with the AXIE model were achieved by employing a space marching method in combination with an immersed boundary method.

3.1.1 Overpressure distribution

Figure 3 shows the overpressure distribution around the AXIE model. The distribution was comparable regardless of the grid resolution; thus, only the result obtained by the fine grid is shown in Fig. 3. The AXIE model was designed in order that the pressure signature generated from the body roughly between $x/L = 0-1.5$ is similar to that from the C25F aircraft. Therefore, the waves issued from the body at $x/L > 1.5$ is not evaluated in this study, as well as in the SBPW. Multiple waves are generated from the AXIE model. This is because the cross-sectional area of the AXIE model are composed of wing, body, tail, nacelle, and flow-through engine. The multiple waves that propagate over $r/L = 5$ shown in Fig. 3 are well captured on square Cartesian grids in a space marching manner. These results show that the complex axisymmetric geometries were well considered as the immersed boundaries developed for the space marching solver in this study.

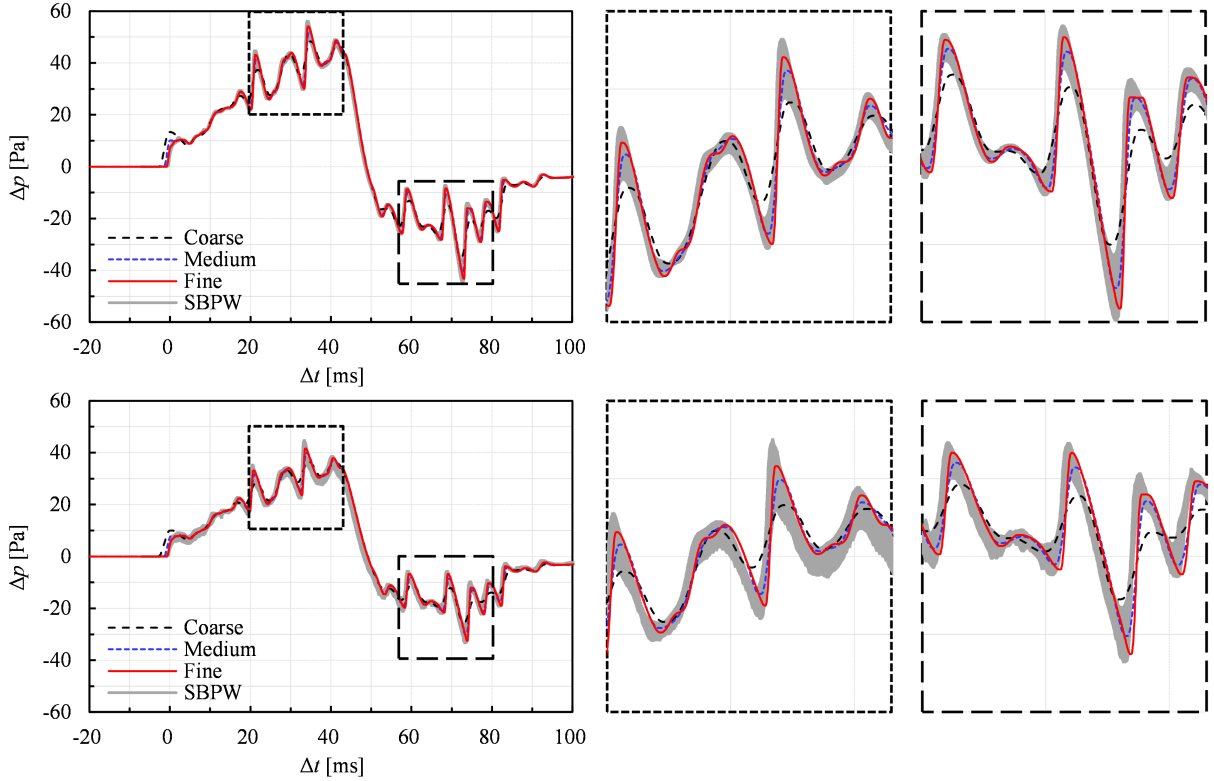


Figure 4: Pressure signature emanating from the AXIE model at $r/L = 3$ (top) and 5 (bottom), obtained by axisymmetric simulation with immersed boundaries for space marching. The results obtained in the SBPW are shown, consisting of the ensemble mean of the results gathered in the SBPW and one standard deviation.

3.1.2 Pressure signature

Figure 4 shows the pressure signature at $r/L = 3$ and 5. The computational accuracy was validated through comparison with the results obtained in the SBPW, which consist of the ensemble mean of the results gathered in the SBPW and one standard deviation. All the computational results in the SBPW were obtained using the conventional time marching methods, not a space marching method. The standard deviation at $r/L = 5$ is higher than that at $r/L = 3$. This is because the grid resolution is deteriorated as the radial distance increases. The pressure signature consists of multiple waves emanating from the complex AXIE geometry shown in Fig. 3. The overpressure is increased as the grid resolution is increased. The trend of grid convergence can be seen through comparison of the results between the coarse, medium, and fine grids. The results obtained by the fine grid lie entirely within the range of one standard deviation obtained in the SBPW. Therefore, the CFD simulations using a space marching method in combination with an immersed boundary method achieve a comparable level of accuracy to those using conventional time marching methods. These results show that the immersed boundary method developed in this study is applicable for evaluating complex axisymmetric geometries which have been difficult to analyze in a space marching manner to date.

3.2 Three-dimensional Simulation of Flows around a Delta Wing Body

Three-dimensional simulation was performed to demonstrate that a Delta Wing Body (DWB) can be resolved using an immersed boundary method for space marching solvers in this section. The DWB was used in the first AIAA SBPW [16], where the near-field pressure signatures gathered from many participants and those obtained from the wind tunnel experiments were provided. The DWB used in the SBPW was the small scale model that was made for the wind tunnel experiments. It consists of an axisymmetric body with the length of $L = 0.1752$ m and a diamond airfoil with the half span of 0.0345 m. The sting used in the wind tunnel experiment is attached to the tail end of the DWB. There are steps in the sting where subsonic flows arise. This violates the requirement of supersonic conditions in a space marching method. Therefore, the sting where $x/L \geq 1$ was replaced by the uniform cylinder with

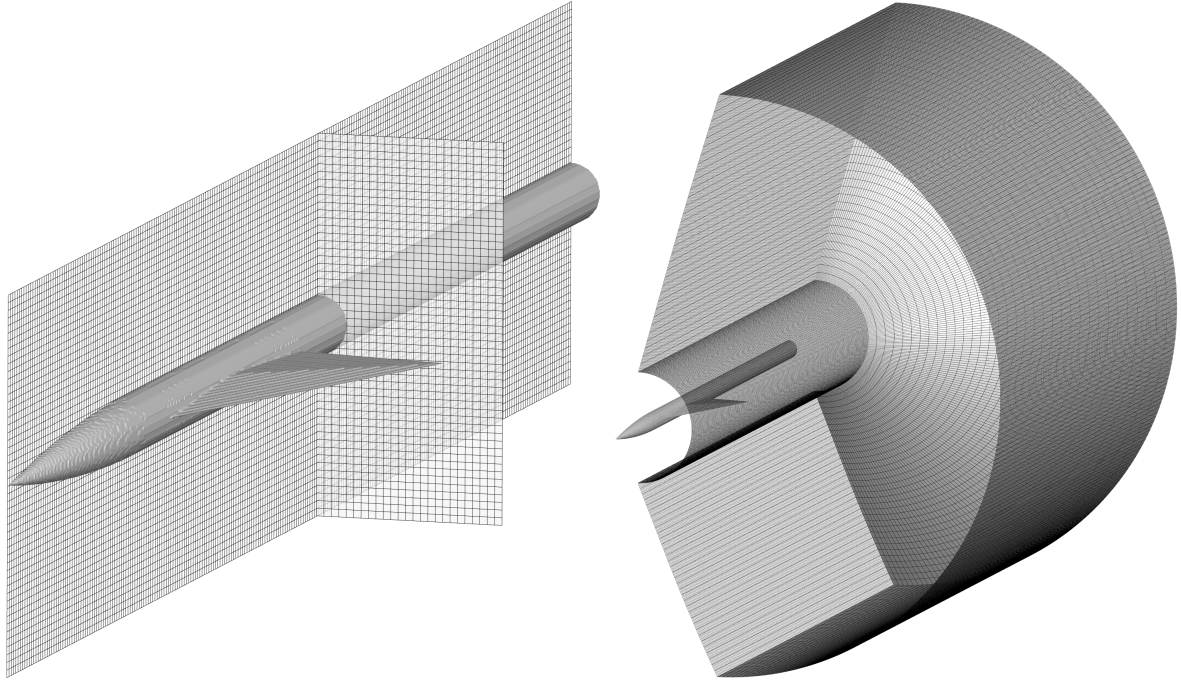


Figure 5: Coarse Cartesian grid (left) in the region of interest around the DWB shown every other points in all directions, and semi-adapted structured grid (right) between $r/L = 0.2$ and 1 shown every 10 points in the x direction.

Table 2: Overview of Cartesian grids used for three-dimensional simulation in the vicinity of the DWB. The region of interest is entirely discretized by grids with the minimum grid spacing, whose number is shown in brackets.

Grid	Minimum grid spacing			Number of grid points			Computational time [s]
	$\Delta x/L$	$\Delta y/L$	$\Delta z/L$	x direction	y direction	z direction	
Coarse	0.004			503	133(53)	265(105)	4.0
Medium	0.002			1005	185(105)	369(209)	14.7
Fine	0.001			2009	289(209)	577(417)	60.1

the diameter of the original sting at $x/L = 1$ in this study. The computational conditions were set to those used in the SBPW. The freestream Mach number was 1.7, and zero angle of attack was assumed.

The three-dimensional steady Euler equations given by Eq. (1) were solved by employing a space marching method. To reduce the computational cost, the computational domain was split into the near field involving the DWB on Cartesian grids and the mid field on semi-adapted structured grids [2]. Figure 5 shows the Cartesian and semi-adapted grids. For the near field simulation, the computational domains in the y and z directions were set between $y/L = 0-5$ and $z/L = -5-5$, respectively. The region of interest in the y and z directions ranged between $y/L = 0-0.2$ and $z/L = -0.2-0.2$, respectively, where high resolution grids were applied. The other region was added for avoiding the influence of the outer boundaries on the region of interest. The grid spacing was increased as the distance from the body increased. The computational domain in the x direction, i.e. the space marching direction, was set to $x/L = -0.008-2.0$. The computational domain was discretized by Cartesian grids shown in Fig. 5. The DWB was evaluated as immersed boundaries which were developed for the space marching solver in this study. The boundary conditions at $x = x_{\min}$, $y = y_{\max}$, $z = z_{\min}$, and $z = z_{\max}$ were set to the freestream condition. The boundary condition at $x = x_{\max}$ is not required for space marching solvers. The symmetric boundary condition was applied at $y = 0$. Table 2 shows the number of grid points and the computational time on a laptop with Intel Core™ i7-1255U (10 cores). The three-dimensional flow simulation around the DWB took only a minute even when the fine grid with approximately 0.34 billion points was used; thus, the fast three-dimensional CFD simulation was achieved using the space marching method in combination with the immersed boundary method. The computational results were comparable between the coarse, medium, and fine grids (see Sec. 3.2.2 for details). Hence, the results

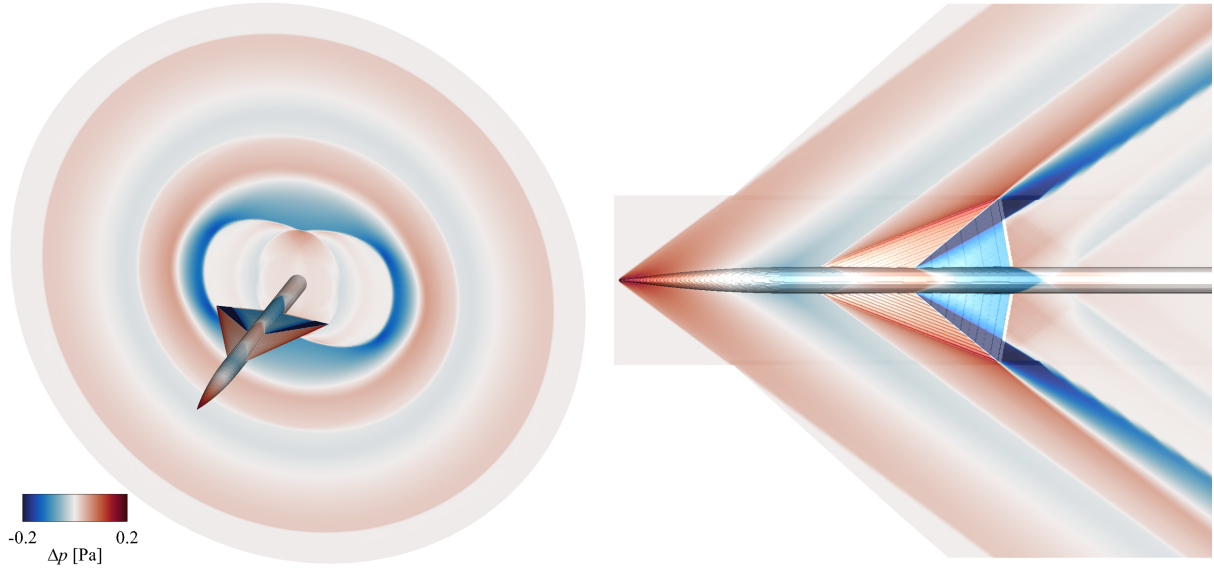


Figure 6: Overpressure distribution around the DWB model, obtained by three-dimensional simulation with immersed boundaries which are applicable for space marching solvers. (left: three-dimensional view, right: bottom view)

obtained by the fine grid are shown in the rest of this paper, unless otherwise stated.

The mid field simulation was performed using semi-adapted structured grids in generalized curvilinear coordinates, where grid lines are aligned to shock waves under restriction of CFL and supersonic conditions that are required for space marching solvers. The cylindrical computational domain was set between $r/L = 0.2-5$. The region of interest ranged between $r/L = 0.2-3.6$. The other region was set for avoiding the influence of the outer boundary on the region of interest. The computational domain in the azimuthal direction was set between $\theta = 0-180^\circ$, considering the symmetry of the DWB. To efficiently capture shock waves, grid lines need to be aligned to their waves. However, in a space marching method, grid topology is restricted due to requirement of CFL and supersonic conditions, as given by Eq. (8); thus, grid lines cannot be strictly aligned to shock waves when using a space marching method. Therefore, a semi-adapted grid was generated as in the previous computational study [2]. The procedure of the grid generation is described as follows: The initial grid was generated, in which the grid angle was set to the Mach angle. Numerical simulation in the region between $r/L = 0.2-1.0$ was performed using the initial grid. If it diverged, the grid was regenerated by slightly increasing the grid angle. Then, the simulation and the grid regeneration were alternately performed until the simulation was finished without divergence. Consequently, the grid lines were made as close to shock waves as possible, while satisfying CFL and supersonic conditions. It should be noted that the shock wave angle significantly changed between $r/L = 0.2 - 1.0$, whereas at $r/L > 1.0$ it changed slightly with the radial distance. Therefore, the grid angle at $r/L > 1.0$ was set to the constant value. The grid spacing in the radial direction was increased between $r = 0.004$ m and 0.2 m as the radial distance increased. The grid spacing in the streamwise and azimuthal directions were set to $\Delta x = 0.0002$ m and $\Delta\theta = 1.0^\circ$, respectively. The equivalent numbers of grid points in the x , r , and θ directions were 1793, 155, and 183 points, respectively. The grid convergence was investigated by comparison with the result obtained by the finer grid that has double the resolution in all directions. Consequently, the pressure signatures at $r/L = 3.6$ were comparable regardless of the grid resolution; thus, the grid resolution is high enough to accurately analyze shock wave propagation between $r/L = 0.2-3.6$. The boundary condition at $r/L = 0.2$ was set by extrapolating the results obtained by the near-field simulation. The boundary at $x = x_{\min}$ and $r = r_{\max}$ was evaluated as freestream. The boundary condition at $x = x_{\max}$ was not needed for space marching solvers. The symmetric boundaries were applied for $\theta = 0$ and 180° . The grid generation and the numerical simulation took tens of seconds each on the same laptop as used in the near-field simulation. Hence, the total computational time including the grid generation over the near and mid fields between $r/L = 0-5$ took less than 100 s even when the fine grid shown in Table 2 was applied. These results indicate that the fast three-dimensional flow simulation around the DWB was achieved by employing the space marching method in combination with the immersed boundary method.

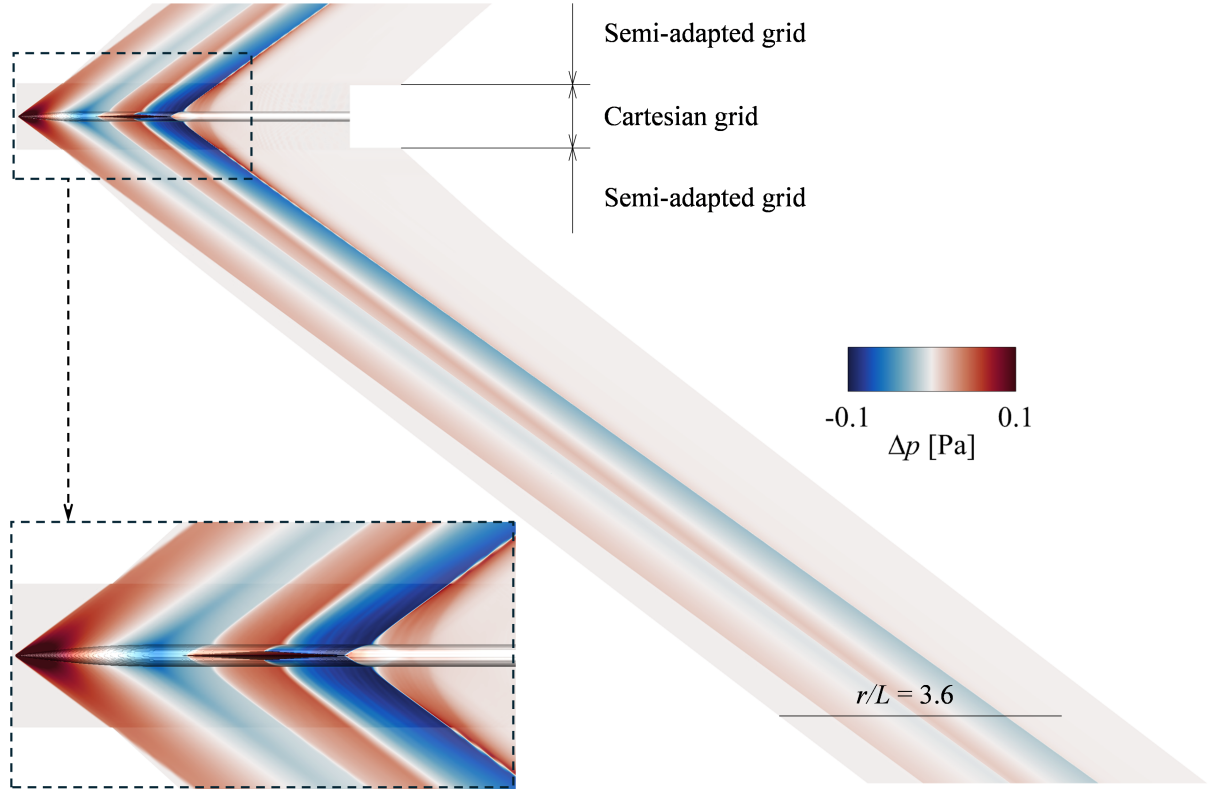


Figure 7: Overpressure distribution from the side view of the DWB, obtained by three-dimensional simulation that uses a space marching method in combination with an immersed boundary method.

3.2.1 Overpressure distribution

Figures 6 and 7 show the overpressure distribution around the DWB. Three shock waves originate from the nose, fore wing, and aft wing, which are hereinafter referred to as the front, middle, and rear shock waves, respectively. They are highly resolved over the entire region of interest between $r/L = 0-3.6$. The interfaces between the Cartesian grids and the semi-adapted grids are smoothly connected. The flow structure is similar to that in the previous computational study [17]. These results demonstrate that the DWB was well evaluated as the immersed boundaries that were applicable for the space marching solver, and the fast simulation involving three-dimensional aircraft geometry was achieved.

3.2.2 Pressure signature

Figure 8 shows the pressure signature at $r/L = 3.6$. The pressure signature consists of the front, middle, and rear shock waves, and the expansion waves between the three shock waves. The abrupt increase due to the shock waves is accurately captured. The overpressure and the locations of the shock waves slightly differ between the coarse, medium, and fine grids. This is mainly because the grid resolution on the immersed boundaries has an effect on the pressure signature. However, the characteristic of the pressure signature is comparable regardless of the grid resolution, and the results indicate a trend toward convergence.

Figure 9 shows the comparison of the pressure signatures between the space marching simulation in this study, the time marching simulation [17], and the wind tunnel experiment [16]. The sting attached to the original DWB was replaced by the uniform cylinder; i.e., the pressure signature behind the rear shock wave differs from those in the time marching simulation and the experiment. The pressure signatures except in the region behind the rear shock wave are comparable in all results, although the overpressure and the locations of the shock waves slightly differ. The previous studies [16] show that the overpressure in the experiment is entirely lower than those in the simulations, and the pressure increase due to the shock waves is gradual; thus, the experimental result has a relatively low resolution. The simulation results gathered in the SBPW differed according to the computational methods. The variation in accuracy among the different computational methods is similar to that observed between the space

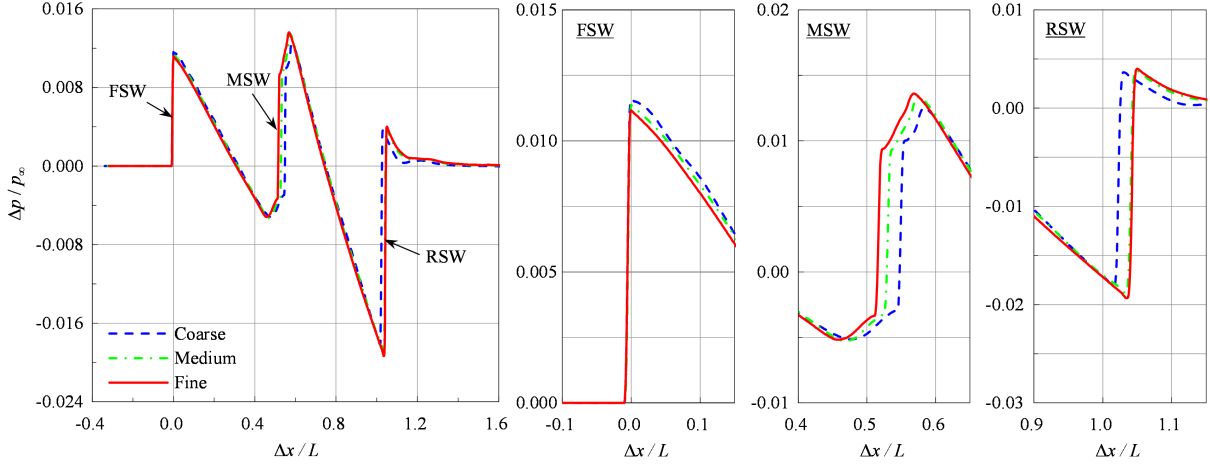


Figure 8: Pressure signature at $r/L = 3.6$ under track of the DWB, obtained by three-dimensional simulation with immersed boundaries which are developed for space marching solvers.

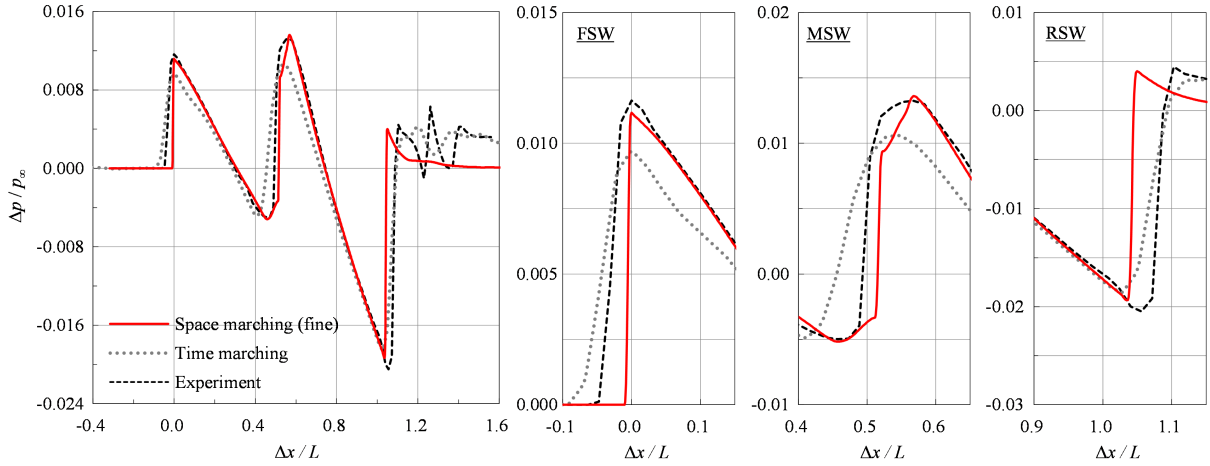


Figure 9: Comparison of pressure signature at $r/L = 3.6$ under track of the DWB model between space marching simulation, time marching simulation [17], and wind tunnel experiment [16].

and time marching methods shown in Fig. 9. Therefore, the three-dimensional simulation using the space marching method with the immersed boundaries reaches a comparable level of accuracy to that using time marching methods. These results demonstrate that the immersed boundary method proposed in this study enables the three-dimensional aircraft geometry to be considered in a space marching manner, while considerably reducing the computational cost.

4 Conclusions

A novel immersed boundary method was developed to consider complex geometries in a space marching manner. Its accuracy was validated through axisymmetric and three-dimensional simulations which respectively dealt with the AXIE model and the DWB on the immersed boundaries. For the axisymmetric simulation, the pressure signature lied entirely within the range of one standard deviation which was obtained in the SBPW. For the three-dimensional simulation, the pressure signatures were comparable to those obtained in the previous simulations using the time marching methods and in the wind tunnel experiments. Therefore, the space marching simulation with the immersed boundaries reached a similar level of accuracy to the time marching simulations; thus, the complex axisymmetric and three-dimensional geometries were successfully considered by employing the immersed boundary method in combination with a space marching method. Furthermore, the three-dimensional flow simulation including the grid generation between $r/L = 0-5$ took less than 100 s on a laptop. These results indicate that the space marching method in combination with the immersed boundary method developed in this study is powerful

for accurately predicting the pressure signature, while considerably reducing the computational cost. This enables parametric studies, which are essential for design of low sonic boom supersonic aircraft, to be conducted more efficiently than ever.

Acknowledgement

This work was supported by the Japan Society for the Promotion of Science (JSPS) KAKENHI Grant Number 21K14349.

References

- [1] Juan J. Alonso and Michael R. Colonno. Multidisciplinary optimization with applications to sonic-boom minimization. *Annual Review of Fluid Mechanics*, 44:505–526, 1 2012.
- [2] Rei Yamashita and Hiroaki Ishikawa. A semi-adapted space marching method for fast sonic boom prediction. *Journal of Computational Physics*, 487, 8 2023.
- [3] Hao Shen and David S. Lazzara. A space marching method for sonic boom near field predictions. *AIAA 2016-2037*, 2016.
- [4] Jeffrey A. Housman, Gaetan K. Kenway, James C. Jensen, and Cetin C. Kiris. Efficient near-field to mid-field sonic boom propagation using a high-order space marching method. *AIAA 2019-3487*, 2019.
- [5] Jared C. Duensing, James C. Jensen, Jeffrey A. Housman, Michael G. Piotrowski, Gaetan K. Kenway, Daniel Maldonado, Emre Sozer, and Cetin C. Kiris. Structured and unstructured simulations for the third aiaa sonic boom prediction workshop. *Journal of Aircraft*, 2021.
- [6] Rei Yamashita, Yoshikazu Makino, and Philip L. Roe. Fast full-field simulation of sonic boom using a space marching method. *AIAA Journal*, 60:4103–4112, 2022.
- [7] Rajat Mittal and Gianluca Iaccarino. Immersed boundary methods. *Annual Review of Fluid Mechanics*, 37:239–261, 2005.
- [8] Charles S. Peskin. The immersed boundary method. *Acta Numerica*, 11:479–517, 1 2002.
- [9] Chi Wang Shu and Stanley Osher. Efficient implementation of essentially non-oscillatory shock-capturing schemes. *Journal of Computational Physics*, 77:439–471, 8 1988.
- [10] B. van Leer. Towards the ultimate conservative difference scheme. iv. a new approach to numerical convection. *Journal of Computational Physics*, 23:276–299, 1977.
- [11] Meng Sing Liou. A sequel to ausm, part ii: Ausm+-up for all speeds. *Journal of Computational Physics*, 214:137–170, 2006.
- [12] Boyce E. Griffith, Richard D. Hornung, David M. McQueen, and Charles S. Peskin. An adaptive, formally second order accurate version of the immersed boundary method. *Journal of Computational Physics*, 223:10–49, 4 2007.
- [13] Fotis Sotiropoulos and Xiaolei Yang. Immersed boundary methods for simulating fluid-structure interaction, 2 2014.
- [14] Yoshiharu Tamaki and Taro Imamura. Turbulent flow simulations of the common research model using immersed boundary method. *AIAA Journal*, 56:2271–2282, 2018.
- [15] Michael A. Park and Marian Nemec. Nearfield summary and statistical analysis of the second aiaa sonic boom prediction workshop. *Journal of Aircraft*, 56:851–875, 2019.
- [16] Michael A. Park and John M. Morgenstern. Summary and statistical analysis of the first aiaa sonic boom prediction workshop. *Journal of Aircraft*, 53:578–598, 2016.
- [17] R. Yamashita and N. Nikiforakis. Three-dimensional full-field simulation of sonic boom emanating from complex geometries over buildings. *Shock Waves*, 33:149–167, 3 2023.